J. Astrophys. Astr. (1982) **3,** 125–144

# Global Stability of Disk-Bulge Systems: Spiral Structure of Disk Galaxies

Ashok Ambastha and Ram K. Varma *Physical Research Laboratory, Navrangpura, Ahmedabad 380009*

Received 1982 January 21; accepted 1982 March 22

**Abstract.** The spiral arms of disk galaxies are very sensitive to various morphological properties, such as, the gas content, the disk-to-bulge ratio *etc.* Here, the stability of self-gravitating annular disks surrounding the central rigid bulge component has been studied in order to explain the transition from the tight spiral arms in Sa galaxies to rather open patterns in Sc galaxies as the central amorphous component diminishes. Smooth spiral patterns are found associated with the dominant (or the fastest growing) modes of the system. When the disk-to-bulge mass ratio is small, a tight pattern results restricted to the inner regions of the disk. This pattern opens up and occupies larger disk areas as the disk component becomes comparable to the bulge. It is found here that the ‘ explosive ‘ instabilities of the global density waves do not occur in the presence of a massive bulge. The growth-rates of the eigen-modes decrease as the disk-to-bulge mass ratio decreases. It is also found that unstable modes of the annular disk can be suppressed by increasing the thermal pressure sufficiently.

*Key words:* global density waves—spiral galaxies—disk-bulge systems

## 1. Introduction

The density-wave theory has been the most successful approach in explaining the spiral structure of disk galaxies (Lin and Shu 1964, 1966; Lin, Yuan and Shu 1969). However, these ‘local’ density-wave theories are based on asymptotic approximations and face severe theoretical difficulties, *viz.* the anti-spirality (Lynden-Bell and Ostriker 1967; Shu 1970) and the problem of radial propagation of these waves (Toomre 1969). These problems can be removed to some extent by invoking certain excitation mechanisms for the density waves (Kato 1970; Mark 1977; Ambastha

and Varma 1978; Bertin and Mark 1978) and, alternatively, by considering the non-linear effects on the local density waves (Norman 1978).

Such asymptotic theories, which are essentially based on the assumption of tightly wrapped spiral waves, are obviously inappropriate for the study of galactic systems having rather open spiral structures. In fact, even the origin of the spiral structure remains unclear, as these theories assume, *a priori,* the existence of a quasi-stationary spiral structure (QSSS) and then proceed to study its consequences through a dispersion relation. However, there have been some attempts to relax the assumption of tight winding by including the terms of higher order in the asymptotic studies (see the review by Bertin 1980). But, for a complete understanding of the large-scale stability of the disks, a global approach with suitable boundary conditions has to be undertaken (lye 1978; Aoki, Noguchi and Iye 1979; Pannatoni and Lau 1979). Ambastha (1981) has studied the global stability of a large number of flat disk models in the form of an eigen-value problem with increasing central density and thermal energy of the disk. A large number of unstable modes are allowed in cold disks, the fastest-growing mode exhibiting the tightest patterns. As the central condensation increases, modes with smaller growth rates are stabilized. On the other hand, an increase in the thermal energy affects the tight spiral modes more appreciably and stabilizes them. In almost all cold disks, with no thermal or internal energy, there exists a number of 'explosive' modes with large growth-rates as compared to their pattern-frequencies. However, some computer simulations (Hohl 1976), as well as studies of global modes (Takahara 1978) have found that the ' explosive ' instabilities could be suppressed to some extent if extensive halos existed around the flat disk. We find here that a massive central bulge may also have a pronounced effect on the density waves sustained by the annular disk surrounding it.

The central bulge or the spheroidal subsystem of the disk galaxies may vary from a very massive and prominent one as in NGC 4594 to extremely small sizes as in NGC 4565. Also, there are galaxies with essentially no bulge, for instance, NGC 598 and NGC 5204. Though the spiral patterns are the characteristic features of the flat disk component, their physical appearance seems to be governed by the size and the massiveness of the bulge which itself does not exhibit any such features. Sandage, Freeman and Stokes (1970) and Freeman (1970) have discussed the role of the disk-to-bulge ratio in the classification of normal spiral galaxies. The bulges, in fact, comprise of old stars with large random velocities and hence they have a spheroidal spread. They do not possess any significant circular rotation and can be assumed to be rigid and stationary. On the other hand, the disk consists of massive young stars, gas and dust clouds and other population I objects apart from a background distribution of intermediate class of population II stars. The grand spiral arms are delineated by these young objects and appear to originate symmetrically from the edge of the central bulge. These spiral tracers are distributed in a ring within 2 kpc $< r <$ 16 kpc with a peak in density at $r \sim$ 4–6 kpc in our Galaxy. (Gordon and Burton 1976; Stecker 1976; Hart and Pedlar 1976; Kodaira 1974).

Considering such a picture of the disk galaxies we have divided the model under investigation here into two subsystems-*viz*. the fixed, central spherical bulge and the flat disk surrounding it–in order to carry out the stability analysis and to understand the effect of the bulge-to-disk ratio on. the density waves sustained by the annular disk. The problem has been posed as an eigen–value problem and the allowed modes

of oscillation in the plane of disk are obtained under the combined influence of the self-consistent potential of the disk and the external potential contributed by the bulge.

We have considered a wide range of values of the ratio of disk mass to the mass of the bulge and also the ratio of the bulge radius to the radius of the disk. Various components of the disk, like gas, dust and young objects have been assumed to constitute a single averaged smeared-out distribution and hence one-component hydrodynamic equations have been used to describe the dynamics of the material constituting the disk. The surface-density profile considered for the annular disk is of a similar form as that of the radial distribution of the spiral tracers in disk galaxies.

In a mathematically similar attempt, Yabushita (1969) has studied the stability of Saturnian rings against axisymmetric ($m = 0$) perturbations under the potential of the massive planet and determined the ratio of the mass of the rings to the mass of the planet in order that the rings may be stable. However, in the galactic context of the spiral structures, one is interested in the non-axisymmetric ($m \neq 0$) modes in pressureless as well as warm disks.

We consider the basic equations describing the dynamics of the disk in Section 2; the equilibrium of disk-bulge system is defined in Section 3. The stability of the equilibrium state against small amplitude perturbations is formulated in Section 4. Section 5 discusses the results in detail and some conclusions are derived in Section 6.

## 2. Basic equations

In this Section we consider the hydrodynamic equations governing the dynamics of the flat disk around the fixed central bulge. The disk is rotating about an axis perpendicular to its plane and passing through the centre of the bulge. In what follows, we have used the cylindrical coordinates.

The continuity equation of the disk is given by

$$\frac{\partial \sigma}{\partial t} + \frac{1}{r}\frac{\partial}{\partial r}(r\sigma u) + \frac{1}{r}\frac{\partial}{\partial \theta}(\sigma v) = 0 \tag{1.1}$$

where $\sigma(r, \theta, t)$ is the surface-density at a point on the annular disk; $u(r, \theta, t)$ and $v(r, \theta, t)$ are the radial and the azimuthal velocities, which are given by the momentum conservation equations as

$$\frac{\partial u}{\partial t} + u\frac{\partial u}{\partial r} + \frac{v}{r}\frac{\partial u}{\partial \theta} - \frac{v^2}{r} = -\frac{1}{\sigma}\frac{\partial p}{\partial r} + \frac{\partial \Psi_d}{\partial r} + \frac{\partial \Psi_b}{\partial r}, \tag{1.2}$$

$$\frac{\partial v}{\partial t} + u\frac{\partial v}{\partial r} + \frac{v}{r}\frac{\partial v}{\partial \theta} + \frac{uv}{r} = -\frac{1}{r\sigma}\frac{\partial p}{\partial \theta} + \frac{1}{r}\frac{\partial \Psi_d}{\partial \theta}. \tag{1.3}$$

Here, $\psi_d$ $(r, \theta, t)$, $\psi_b$ $(r)$, $p(r, \theta, t)$ represent the self-consistent potential of the disk, the fixed potential exerted by the central bulge and the pressure, respectively.

The gravitational potential of the disk $\psi_d$ $(r, \theta, t)$, corresponding to the surface-density $\sigma(r, \theta, t)$, is given by Poisson's equation

$$\nabla^2 \Psi_d = -4\pi G \delta(z) \sigma(r, \theta, t). \tag{1.4}$$

The term $\partial\psi_b/\partial r$ representing the gravitational force at a point on the disk due to the bulge has been defined in Section 3.

Finally, we assume a polytropic relation for pressure in the form

$$p = c\sigma^{\gamma} \tag{1.5}$$

for the closure of the set of Equations (1.1) – (1.4). Here, $c$ represents a measure of the ' warmness ' of the disk and $\gamma$ is the polytropic index.

## 3. Equilibrium of the disk-bulge system

Let us now consider a general axisymmetric surface-density distribution in a flat annular disk

$$\sigma_0(r) = \sum_{j=0}^{\infty} a_j F_0(\lambda_j^{(0)} r); \quad a \leqslant r \leqslant b$$
$$= 0 \quad ; \quad r > b \text{ and } r < a \tag{2.1}$$

where

$$F_0(\lambda_j^{(0)} r) \equiv J_0(\lambda_j^{(0)} r) + G_j^{(0)} Y_0(\lambda_j^{(0)} r). \tag{2.2}$$

Here, $J_0(x)$ and $Y_0(x)$ are Bessel functions of order zero and $\lambda_j^{(0)}$ denote the roots of the transcendental equation

$$J_0(\lambda a) Y_0(\lambda b) - J_0(\lambda b) Y_0(\lambda a) = 0. \tag{2.3}$$

Also, $G_j^{(0)}$ in Equation (2.2) are defined as

$$G_j^{(0)} = -\frac{J_0(\lambda_j^{(0)} a)}{Y_0(\lambda_j^{(0)} a)} = -\frac{J_0(\lambda_j^{(0)} b)}{Y_0(\lambda_j^{(0)} b)}, \tag{2.4}$$

in order to ensure the vanishing of the surface-density at both the edges of the annular disk, *i.e.* at the inner radius $r = a$, and the outer edge $r = b$.

The roots of Equation (2.3), $\lambda_j^{(0)}$, would depend on the specification of the disk boundary. We have listed the zeros $\lambda_j^{(m)}$ of $F_m(\lambda_j^{(m)} r) = 0$ at $r = a$ in Table 1 for $a/b$ $(\equiv a) = 0{\cdot}25$, $0{\cdot}5$ and $0{\cdot}75$ and $m = 0$ and 2. The functions $F_m(x)$, as constructed according to Equation (2.2), are orthogonal.

Now, any density distribution can be constructed in the form (2.1) by choosing appropriate coefficients of expansion, $a_j$, which can be found by using the orthogo-

**Table 1.** Roots of $F_{jr}^{m} = 0$ at $r = a$ and $r = b$.

| | $m = 0$ | | | $m = 2$ | | |
|---|---|---|---|---|---|---|
| $a/b$ | 0·25 | 0·50 | 0·75 | 0·25 | 0·5 | 0·75 |
| $j$ | | | | | | |
| 1 | 4·097686 | 6·246062 | 12·553266 | 5·319868 | 6·813843 | 12·761297 |
| 2 | 8·323774 | 12·546871 | 25·126130 | 9·144361 | 12·855532 | 25·231701 |
| 3 | 12·528667 | 18·836415 | 37·694697 | 13·121498 | 19·045705 | 37·765274 |
| 4 | 16·726277 | 25·122846 | 50·262169 | 17·184754 | 25·280762 | 50·315154 |
| 5 | 20·920591 | 31·407996 | 62·829202 | 21·292746 | 31·534683 | 62·871609 |
| 6 | 25·113152 | 37·692496 | 75·396014 | 25·425757 | 37·798231 | 75·431362 |
| 7 | 29·304675 | 43·976623 | 87·962700 | 29·573912 | 44·067336 | 87·993003 |
| 8 | 33·495534 | 50·260516 | 100·52931 | 33·731852 | 50·339937 | 100·55582 |
| 9 | 37·685943 | 56·544251 | 113·09586 | 37·896453 | 56·614877 | 113·11943 |
| 10 | 41·876034 | 62·827878 | 125·66238 | 42·065783 | 62·891460 | 125·68360 |
| 11 | 46·065893 | 69·111424 | 138·22887 | 46·238587 | 69·169238 | 138·24816 |
| 12 | 50·255576 | 75·394910 | 150·79534 | 50·414014 | 75·447915 | 150·81302 |
| 13 | 54·445122 | 81·678350 | 163·36180 | 54·591471 | 81·727284 | 163·37812 |
| 14 | 58·634562 | 87·961753 | 175·92824 | 58·770530 | 88·007197 | 175·94340 |
| 15 | 62·823916 | 94·245128 | 188·49468 | 62·950873 | 94·287546 | 188·50882 |

nality of the functions, $F_0\ (\lambda_j^{(0)}\, r)$. Thus, it should suffice here if we consider a particular distribution of the form

$$\sigma_0(r) = a_0\left[J_0(\lambda_0 r) - \frac{J_0(\lambda_0 a)}{Y_0(\lambda_0 a)}\, Y_0(\lambda_0 r)\right]; \quad a \leqslant r \leqslant b$$
$$= \qquad 0 \qquad ; \quad r < a \text{ or } r > b \tag{2.5}$$

where $\lambda_0$ is the smallest root of the Equation (2.3).

The gravitational potential in the plane of the axisymmetric flat disk corresponding to a given surface-density distribution is obtained by using the Hankel transform $A\ (\tilde{\omega})$ of $\sigma_0(r)$ such that

$$A_0(\tilde{\omega}) = \int_0^\infty J_0(\tilde{\omega} r)\, \sigma_0(r)\, r\, dr. \tag{2.6}$$

This can be inverted to obtain

$$\sigma_0(r) = \int_0^\infty J_0(\tilde{\omega} r)\, A_0(\tilde{\omega})\, \tilde{\omega}\, d\tilde{\omega}$$

(*cf.* Clutton-Brock 1972). Correspondingly, the potential is given by

$$\Psi_0(r, z) = 2\pi G \int_0^\infty J_0(\tilde{\omega} r)\, A_0(\tilde{\omega}) \exp(-\tilde{\omega}\,|z|)\, d\tilde{\omega}. \tag{2.7}$$

On substituting for $\sigma_0\ (r)$ from Equation (2.5) in Equation (2.6), one gets

$$A_0(\tilde{\omega}) = \frac{2a_0}{\pi(\tilde{\omega}^2 - \lambda_0^2)}\left[\frac{J_0(\tilde{\omega} a)}{Y_0(\lambda_0 a)} - \frac{J_0(\tilde{\omega} b)}{Y_0(\lambda_0 b)}\right]. \tag{2.8}$$

On substituting for $A_0$ ($\tilde{\omega}$) from Equation (2.8), the gravitational potential in the plane of the disk can be obtained, following Yabushita (1969), as

$$\Psi_0(r) = 2\pi G a_0 \left[ \frac{F_0(\lambda_0 r)}{\lambda_0 b} + \frac{4}{\pi^2} \int_0^\infty \left\{ \frac{I_0(zr) K_0(zb)}{Y_0(\lambda_0 b)} - \frac{I_0(za) K_0(zr)}{Y_0(\lambda_0 a)} \right\} \frac{dz}{(\lambda_0^2 + z^2)} \right] \quad (2.9)$$

where $I_0$ ($x$) and $K_0$ ($x$) are modified Bessel functions of first and second kind and order zero.

The equation of continuity (1.1) and the azimuthal component of the momentum conservation equation (1.3) are satisfied identically for the axisymmetric equilibrium disk, while the radial component of the momentum conservation equation (1.2) yields the rotational velocity of the disk as

$$-r\Omega_0^2 \equiv -\frac{V_0^2}{r} = -\frac{1}{\sigma_0}\frac{dP_0}{dr} - \frac{GM_b}{r^2} + \frac{d\Psi_d}{dr}, \quad (2.10)$$

where $M_b$ denotes the mass of the central spherical bulge. Here, $GM_b/r^2$ is the external gravitational force exerted by the fixed bulge and $d\psi_d/dr$ represents the self-consistent potential of the disk component. The azimuthal velocity, $V_0(r)$, can thus be obtained by Equation (2.10) once the nature of the pressure force is specified.

Now, we define the non-dimensional quantities $\hat{\sigma}(\xi)$, $\hat{\psi}(\xi)$ *etc.* such that

$$\Psi(r) = (\pi GM/b)\,\hat{\Psi}(\xi),$$

$$\sigma(r) = (M/2\pi b^2)\,\hat{\sigma}(\xi),$$

$$P(r) = (GM^2/2b^3)\,\hat{P}(\xi)$$

and

$$V_0(r) = (\pi GM/b)^{1/2}\,\hat{V}_0(\xi), \quad (2.11)$$

where $\xi = r/b$.

Thus, using the definitions (2.11) in Equation (2.10), we get the non-dimensional radial equation of motion

$$\frac{\hat{V}_0^2(\xi)}{\xi} = \frac{1}{\hat{\sigma}_0(\xi)}\frac{d\hat{P}_0(\xi)}{\partial\xi} + \frac{1}{\pi(1+\beta)}\cdot\frac{1}{\xi^2} - \frac{d\hat{\Psi}_d(\xi)}{d\xi} \quad (2.12)$$

where the net mass of the system is

$$M = M_d + M_b$$

and $\beta = M_d/M_b$.

The surface-density profiles for various values of the disk-to-bulge mass ratio ($\equiv \beta$) are shown in Fig. 1. As the mass of the bulge decreases, the mass of the disk increases so as to keep the net mass $M$ fixed. In all these cases, the ratio of the inner and the outer radii is kept constant at $\alpha = 0{\cdot}25$. The circular-velocity profile is only slightly altered if $\beta$ is varied. Fig. 2 exhibits the surface-density and rotational profiles for $\beta = 0{\cdot}2$ and various values of $\alpha$.

It should be noted here that, for a physical and realistic disk, the following criteria should be satisfied throughout the disk

$$\Omega_0^2(\xi) \geqslant 0, \tag{2.13a}$$

$$K_0^2(\xi) \equiv 2\Omega_0\left[2\Omega_0 + \xi\frac{d\Omega_0}{d\xi}\right] \geqslant 0 \tag{2.13b}$$

and

$$\frac{d\Omega_0(\xi)}{d\xi} \leqslant 0, \tag{2.13c}$$

$\Omega_0$ and $K_0$ being the angular and epicyclic frequencies, respectively.

Here, the disks do not satisfy the condition (2.13a) when $\alpha \geqslant 0{\cdot}75$ and $\beta > 0{\cdot}5$. The condition (2.13c) also does not hold good for disks with $\alpha \geqslant 0{\cdot}75$. Table 2 shows the azimuthal velocities at the inner and the outer edges of the disk for some values of the parameters $\alpha$ and $\beta$.

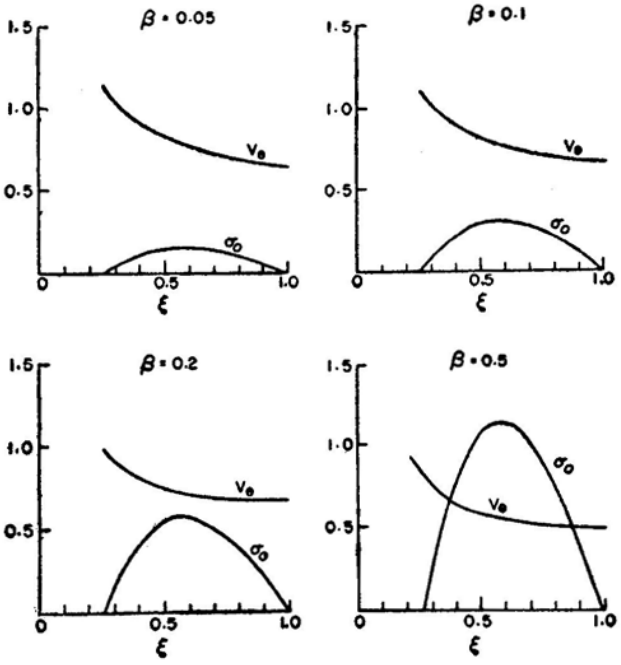


**Figure 1.** The radial profiles of surface density and circular velocity for various values of $M_d/M_b$ and $a/b = 0{\cdot}25$.

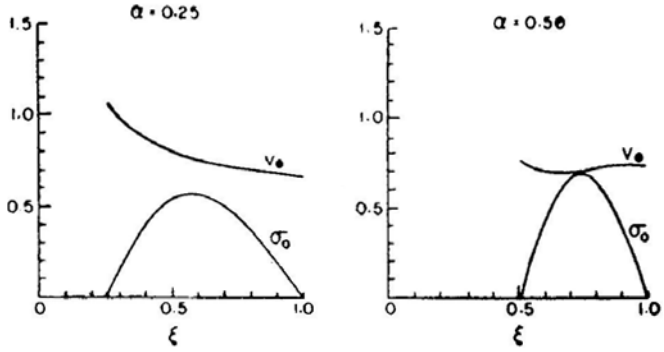


**Figure 2**. The radial profiles of surface density and circular velocity for two values of inner-to-outer radii of the disk and $M_d/M_b = 0{\cdot}20$.

## 4. Normal mode analysis of the perturbed disk

We consider an infinitesimally small perturbation in the gravitational potential of the annular disk, which in turn perturbs the surface density, velocity *etc.* of the equilibrium disk (as defined in Section 3). Since the boundaries of the disk are free to move, we now have

$$a(\tau) = a + \epsilon_a(\tau)$$

and

$$b(\tau) = b + \epsilon_b(\tau), \tag{3.1}$$

for the inner and the outer radii of the perturbed disk. Here, $\varepsilon_a$ and $\varepsilon_b$ are some small quantities of first order in the perturbation. One can linearize the basic hydrodynamic equations (1.1)—(1.5) governing the system and obtain the following set of equations for the perturbed quantities:

$$\left(\frac{\partial}{\partial\tau} + \frac{V_0}{\xi}\frac{\partial}{\partial\theta}\right)\tilde{\sigma} + \frac{1}{\xi}\left[\frac{\partial}{\partial\xi}(\xi\,\sigma_0\,\tilde{u}) + \frac{\partial}{\partial\theta}(\sigma_0\,\tilde{v})\right] = 0, \tag{3.2}$$

**Table 2.** Circular velocities for disk-bulge systems at inner and outer edges of the disk.

| $\alpha$ | 0·25 | | 0·50 | | 0·75 | |
|---|---|---|---|---|---|---|
| $\beta$ | $V(a)$ | $V(b)$ | $V(a)$ | $V(b)$ | $V(a)$ | $V(b)$ |
| 0·40 | 1·045 | 0·737 | 0·748 | 0·843 | 0·318 | 1·000 |
| 0·50 | 1·030 | 0·762 | 0·740 | 0·881 | 0·217 | 1·000 |
| 0·75 | 1·000 | 0·810 | 0·722 | 0·952 | | |
| 1·00 | 0·977 | 0·843 | 0·709 | 1·002 | | |
| 1·50 | 0·944 | 0·889 | 0·690 | 1·068 | | |
| 2·00 | 0·921 | 0·918 | 0·677 | 1·111 | | |
| 2·50 | 0·905 | 0·938 | 0·667 | 1·39 | | |
| 3·00 | 0·892 | 0·953 | 0·660 | 1·61 | | |

Unphysical disk

Note:

The condition $\dfrac{d\Omega_0(\xi)}{d\xi} < 0$ does not hold inside the box.

$$\left(\frac{\partial}{\partial \tau}+\frac{V_0}{\xi}\frac{\partial}{\partial \theta}\right)\tilde{u}-\frac{2V_0}{\xi}\tilde{v}=-\frac{1}{\sigma_0}\frac{\partial \tilde{p}}{\partial \xi}+\frac{\tilde{\sigma}}{\sigma_0^2}\frac{dP_0}{d\xi}+\frac{\partial \tilde{\psi}_d}{\partial \xi}, \tag{3.3}$$

$$\left(\frac{\partial}{\partial \tau}+\frac{V_0}{\xi}\frac{\partial}{\partial \theta}\right)\tilde{v}+\left(\frac{V_0}{\xi}+\frac{dV_0}{d\xi}\right)\tilde{u}=\frac{1}{\xi}\left[-\frac{1}{\sigma_0}\frac{\partial \tilde{p}}{\partial \theta}+\frac{\partial \tilde{\psi}_d}{\partial \theta}\right], \tag{3.4}$$

where $\tilde{\sigma}(\xi, \theta, \tau)$, $\tilde{u}(\xi, \theta, \tau)$, $\tilde{v}(\xi, \theta, \tau)$, $\tilde{P}(\xi, \theta, \tau)$, $\tilde{\psi}_d(\xi, \theta, \tau)$ are perturbed density, velocities, pressure and potential, respectively and $\tau$ is a non-dimensional time, given by

$$\tau = (\pi G M/R^3)^{1/2} t.$$

The bulge being rigid and stationary, the perturbations of the bulge density *etc.* have been neglected and hence it does not contribute to the perturbed equations apart from influencing the rotational profile of the system.

Since the equilibrium density distribution, $\sigma_0(\xi)$, is redistributed due to a perturbation in the gravitational potential, which itself corresponds to a small density perturbation, $\sigma_1(\xi, \theta, \tau)$, the net surface density of the annular disk can be written as

$$\sigma(\xi, \theta, \tau) = a_0 F_0(\Lambda_0 \xi) + \sigma_1(\xi, \theta, \tau) \tag{3.5}$$

where $\Lambda_0$ is the smallest root of the transcendental equation

$$F_0(\Lambda_0 \xi) \equiv J_0(\Lambda_0 \xi) + G^{(0)} Y_0(\Lambda_0 \xi) = 0 \tag{3.6}$$

at $\xi = a(\tau)$ and $\xi = b(\tau)$. Let us write

$$a_0 F_0(\Lambda_0 \xi) - a_0 F_0(\lambda_0 \xi) = \epsilon \sum_{k=0}^{\infty} D_k F_m(\lambda_k^{(m)} \xi), \tag{3.7}$$

where $\lambda_k^{(m)}$ are the roots of the equation

$$J_m(\lambda) Y_m(\lambda a) - J_m(\lambda a) Y_m(\lambda) = 0$$

and where

$$F_m(\lambda_k^{(m)} \xi) \equiv J_m(\lambda_k^{(m)} \xi) + G_k^{(m)} Y_m(\lambda_k^{(m)} \xi)$$

with $G_k^{(m)} = -J_m(\lambda_k^{(m)} a)/Y_m(\lambda_k^{(m)} a)$.

Similarly, one can also expand the perturbed density, $\sigma_1(\xi, \theta, \tau)$ as

$$\sigma_1(\xi, \theta, \tau) = \epsilon \sum_{k=0}^{\infty} E_k F_m(\lambda_k^{(m)} \xi). \tag{3.8}$$

Here,

$$\epsilon(\theta, \tau) = \epsilon_0 \exp[i(\omega\tau + m\theta)].$$

Thus the net surface density in the disk is

$$\sigma(\xi, \theta, \tau) = a_0 F_0(\lambda_0 \xi) + \epsilon \sum_{k=0}^{\infty} C_k F_m(\lambda_k^{(m)} \xi) \equiv \sigma_0(\xi) + \tilde{\sigma}(\xi, \theta, \tau) \tag{3.9}$$

where we have defined $C_k = E_k + D_k$ which is to be determined later. Now, the potential $\hat{\psi}_{\kappa}^{(m)}(\xi)$ corresponding to the surface-density distribution $F_m(\lambda_{\kappa}^{(m)} \xi)$ can be written in a non-dimensional form as

$$\hat{\psi}_k^{(m)}(\xi) = \frac{1}{\pi}\left[\frac{F_m(\lambda_k^{(m)} \xi)}{\lambda_k^{(m)}} + \frac{4}{\pi^2}\int_0^{\infty}\left\{\frac{I_m(z\xi) K_m(z)}{Y_m(\lambda_k^{(m)})} - \frac{I_m(za) K_m(z\xi)}{Y_m(\lambda_k^{(m)} a)}\right\}\frac{dz}{z^2 + \lambda_k^{(m)2}}\right] \tag{3.10}$$

as in Equation (2.9). The net potential is hence

$$\Psi(\xi, \theta, \tau) = \Psi_0(\xi) + \tilde{\Psi}(\xi, \theta, \tau) \tag{3.11}$$

$$\text{with} \qquad \tilde{\Psi}(\xi, \theta, \tau) = \epsilon \sum_{k=0}^{\infty} C_k \hat{\psi}_k^{(m)}(\xi).$$

Considering the azimuthal and the time dependence of the form

$$\tilde{A}(\xi, \theta, \tau) = \hat{A}(\xi) \exp[i(\omega\tau + m\theta)] \tag{3.12}$$

for all the perturbed quantities, and by adding to and subtracting from Equation (3.3) $i$ times Equation (3.4), one obtains

$$i\omega(\hat{u} - i\hat{v}) + i(m-1)\frac{V_0}{\xi}(\hat{u} - i\hat{v}) - \frac{V_0}{\xi}\hat{v} - i\hat{u}\frac{dV_0}{d\xi}$$

$$= -\frac{1}{\sigma_0}\left\{\frac{d\hat{p}}{d\xi} + \frac{m}{\xi}\hat{p}\right\} + \frac{\hat{\sigma}}{\sigma_0^2}\frac{dP_0}{d\xi} + \left\{\frac{d\hat{\psi}}{d\xi} + \frac{m}{\xi}\hat{\psi}\right\}, \tag{3.13}$$

$$i\omega(\hat{u} + i\hat{v}) + i(m+1)\frac{V_0}{\xi}(\hat{u} + i\hat{v}) - \frac{V_0}{\xi}\hat{v} + i\hat{u}\frac{dV_0}{d\xi}$$

$$= -\frac{1}{\sigma_0}\left\{\frac{d\hat{p}}{d\xi} - \frac{m}{\xi}\hat{p}\right\} + \frac{\hat{\sigma}}{\sigma_0^2}\frac{dP_0}{d\xi} + \left\{\frac{d\hat{\psi}}{d\xi} - \frac{m}{\xi}\hat{\psi}\right\} \tag{3.14}$$

and

$$i\left(\omega+\frac{m}{\xi}V_0\right)\hat{\sigma}+\frac{1}{\xi}\frac{d}{d\xi}(\xi\,\sigma_0\,\hat{u})+i\frac{m}{\xi}\sigma_0\,\hat{v}=0. \tag{3.15}$$

And the perturbed pressure $\hat{p}\,(\xi)$ in Equations (3.13) and (3.14) is given by

$$\hat{p}(\xi)=\frac{\gamma P_0(\xi)}{\sigma_0(\xi)}\hat{\sigma}(\xi), \tag{3.16}$$

using Equation (1.5).

We expand the perturbed quantities $\hat{u}-i\hat{v}$ and $\hat{u}+i\hat{v}$ as

$$\hat{u}-i\hat{v}=i\sum_{k=0}^{\infty}A_k\,F_{m-1}\,(\lambda_k^{(m)}\,\xi) \tag{3.17}$$

and

$$\hat{u}+i\hat{v}=i\sum_{k=0}^{\infty}B_k\,F_{m+1}\,(\lambda_k^{(m)}\,\xi) \tag{3.18}$$

where the coefficients of expansion $A_k$, $B_k$ are to be determined. Substituting the expansions for the perturbed quantities from the Equations (3.9), (3.11), (3.16)–(3.18) in the set of Equations (3.13)–(3.15) and carrying out the necessary simplifications, one obtains the following equations:

$$\sum_{k=0}^{\infty}\Big[A_k\cdot\tfrac{1}{2}\{F_{m-1}\,(\lambda_k\,\xi)\,\sigma_0'-\lambda_k\,F_m\,(\lambda_k\,\xi)\,\sigma_0\}+B_k\cdot\tfrac{1}{2}\{F_{m+1}\,(\lambda_k\,\xi)\,\sigma_0'$$
$$+\lambda_k\,F_m\,(\lambda_k\,\xi)\,\sigma_0\}+C_k\left\{\omega+\frac{m}{\xi}V_0\right\}F_m\,(\lambda_k\,\xi)\Big]=0, \tag{3.13a}$$

$$\sum_{k=0}^{\infty}\left[A_k\left\{-\left(\omega-\frac{m-1}{\xi}V_0\right)+\frac{1}{2}\left(\frac{V_0}{\xi}+V_0'\right)\right\}F_{m-1}\,(\lambda_k\,\xi)+B_k\left\{\frac{1}{2}\left(V_0'-\frac{V_0}{\xi}\right)\right\}\right.$$
$$\times F_{m+1}\,(\lambda_k\,\xi)+C_k\left\{-\left(\frac{\gamma P_0}{\sigma_0^2}\lambda_k+\frac{1}{\pi}\right)F_{m-1}\,(\lambda_k\,\xi)-\frac{\gamma\,(\gamma-2)}{\sigma_0^3}P_0\,\sigma_0'\,F_m\,(\lambda_k\,\xi)\right.$$
$$\left.\left.-\frac{4}{\pi^3}\mathbf{L}_k^{(m-1)}\,(\xi)\right\}\right]=0 \tag{3.14a}$$

and

$$\sum_{k=0}^{\infty}\left[A_k\left\{\frac{1}{2}\left(\frac{V_0}{\xi}-V_0\right)\right\}F_{m-1}\,(\lambda_k\,\xi)+B_k\left\{-\left(\omega+\frac{m+1}{\xi}V_0\right)\right.\right.$$
$$-\frac{1}{2}\left(\frac{V_0}{\xi}+V_0'\right)\Big\}F_{m+1}\,(\lambda_k\,\xi)+C_k\left\{-\left(\frac{\gamma\,P_0}{\sigma_0^2}\lambda_k-\frac{1}{\pi}\right)F_{m+1}\,(\lambda_k\,\xi)\right.$$
$$\left.\left.+\frac{\gamma\,(\gamma-2)\,P_0\,\sigma_0'}{\sigma_0^3}F_m\,(\lambda_k\,\xi)-\frac{4}{\pi^3}\mathbf{L}_k^{m+1}\,(\xi)\right\}\right]=0 \tag{3.15a}$$

where we have defined

$$\mathbf{L}_k^{(m-1)}(\xi) = \int_0^\infty \frac{z\,dz}{\lambda_k^2 + z^2} \left\{ \frac{I_{m-1}(z\xi)\, K_m(z)}{Y_m(\lambda_k)} + \frac{I_m(z\alpha)\, K_{m-1}(z\xi)}{Y_m(\lambda_k\, \alpha)} \right\} \tag{3.19}$$

and

$$\mathbf{L}_k^{(m+1)}(\xi) = \int_0^\infty \frac{z\,dz}{\lambda_k^2 + z^2} \left\{ \frac{I_{m+1}(z\xi)\, K_m(z)}{Y_m(\lambda_k)} + \frac{I_m(z\alpha)\, K_{m+1}(z\xi)}{Y_m(\lambda_k\, \alpha)} \right\}. \tag{3.20}$$

In all the above equations, we have dropped the superscript $m$ from the roots $\lambda_k^{(m)}$ for brevity.

Now, we multiply the Equations (3.13a)–(3.15a) by $\xi F_m(\lambda_j \xi)$, $\xi F_{m-1}(\lambda_j \xi)$ and $\xi F_{m+1}(\lambda_j, \xi)$, respectively and integrate the resulting equations over the annular disk in the interval $(\alpha, 1)$ to get an infinite s et of algebraic equations:

$$\sum_{k=0}^{\infty} [A_k\, P_{kj} + B_k\, Q_{kj} + C_k\, R_{kj}] = \omega\, A_j, \tag{3.13b}$$

$$\sum_{k=0}^{\infty} [A_k\, S_{kj} + B_k\, T_{kj} + C_k\, U_{kj}] = \omega\, B_j, \tag{3.14b}$$

$$\sum_{k=0}^{\infty} [A_k\, V_{kj} + B_k\, W_{kj} + C_k\, X_{kj}] = \omega\, C_j, \tag{3.15b}$$

with the coefficients $P_{kj}$, $Q_{kj}$ *etc*. as defined in Appendix. Equations (3.13b)–(3.15b) can conveniently be written in a matrix from as an eigen-value problem

$$\begin{bmatrix} P & Q & R \\ S & T & U \\ V & W & X \end{bmatrix} \begin{bmatrix} A \\ B \\ C \end{bmatrix} = \omega \begin{bmatrix} A \\ B \\ C \end{bmatrix} \tag{3.21}$$

or $\quad MZ = \omega Z$

where $P$, $Q$, $R$, .. represent infinite-dimensional matrices and $M$, consequently, is a $3\infty \times 3\infty$ matrix. Equation (3.21) is an eigen-value value problem for the perturbations $\tilde{\sigma}(\xi, \theta, \tau)$, $\tilde{\psi}(\xi, \theta, \tau)$ *etc*. in the plane of the disk with the $\omega$ as the eigen-values and $Z\ \{\equiv (A, B, C)^\dagger\}$ representing corresponding eigen-functions.

The matrix $M$ is real and, in general, is non-symmetric. Hence, the eigen-value problem would permit real and/or complex conjugate pairs of eigen-values. The complex eigen-modes will be associated with complex eigen-functions, contributing radial phase shifts in the location of the maxima of the perturbations. Thus, the complex eigen-modes may naturally allow spiral patterns in the disk. This result—

that only complex modes admit spiral patterns—confirms the 'antispiral' theorem according to which no spiral waves are allowed to be associated with the neutral (or, purely oscillatory) modes

It is impossible to solve the eigen-value problem given by Equation (3.21) as it stands, with infinite-dimensional matrices, and suitable truncated forms of $M$ and Z have to be employed. Of course, the convergence of the resulting modes of oscillations is to be ensured.

In order to study the eigen-patterns associated with the perturbations in a satisfactory way, we have plotted here the amplitudes of the perturbation, say, the surface density perturbation, at a large number of points, in-and out-side the annular disk boundaries. The results have been presented in a three-dimensional form.

## 5. Results and discussion

In this Section, we discuss the results of the eigen-value problem for the stability of the annular disk under the combined influence of the external field of the central bulge and the collective field of the disk. The surface density adopted vanishes at both the boundaries. In fact, such a density distribution represents the young objects, *viz.* the spiral tracers in galactic disks, which are only a small fraction of the total mass of the disk. Thus, we have ignored the background population of the intermediately old population II stars which have an exponential distribution in the disk. However, we have already investigated the problem of the stability of disks where the collective effects of the entire system has been considered (Ambastha 1981). Here, our interest lies mainly in the study of the effects of a fixed bulge component on the density waves sustained by the gaseous disk. For this reason, and also to avoid the presence of the singularities at the edges, we have considered that the density vanishes at the boundaries. In a separate paper, we would consider the effect—on the density waves in the disk—of the field generated by a static distribution of the old population II stars in the disk besides that due to the central bulge.

Here, all the eigenvalues, real as well as complex, corresponding to a truncated $N \times N$ matrix are obtained by using similarity transformation method for the evaluation of the eigen-value problem. The real modes exhibit spoke-like features because of the fact that the neutral modes do not yield radial phase shifts, which would otherwise be contributed by the imaginary part of the eigen-functions in the case of the complex modes. Thus, only the complex modes may provide spirals, and only those which are associated with unstable modes would survive in the disk. For this reason, we have considered here only the growing modes in detail. Since the matrix $M$ is nonsymmetric, with no regular or well-defined variations in the magnitude of the matrix elements away from the diagonal, it is not possible to evaluate, exactly, all the eigen-values and the associated eigen-functions of the truncated matrix. As the dimension of the truncated matrix is increased, one expects to refine the eigen-modes; however, the numerical errors start becoming significant for larger matrices and hence one cannot increase the dimension of the matrix without limit. We have considered here in most cases, matrices of the order of $45 \times 45$. Only those modes have been discussed which exhibit a reasonable convergence and the rest of them are ignored while discussing the spiral patterns.

**Table 3**. The principal mode for various disk-bulge models (cold disk).

| $\alpha$ | 0·25 | | 0·5 | | 0·75 | |
|---|---|---|---|---|---|---|
| $\beta$ | $\omega_r$ | $-\omega_i$ | $\omega_r$ | $-\omega_i$ | $\omega_r$ | $-\omega_i$ |
| 0·02 | 1·9844 | 0·2278 | No unstable mode exists | | No unstable mode exists | |
| 0·10 | 1·8188 | 0·2278 | | | | |
| 0·25 | 1·6954 | 0·2604 | | | | |
| 0·40 | 1·5659 | 0·2931 | 1·3427 | 0·0160 | 0·8287 | 0·0333 |
| 0·50 | 1·5231 | 0·2950 | 1·3343 | 0·0366 | 0·7215 | 0·0521 |
| 0·75 | 1·4386 | 0·2881 | 1·3212 | 0.0601 | Unphysical disks | |
| 1·00 | 1·3650 | 0·2820 | 1·3166 | 0·0697 | | |
| 1·50 | 1·2909 | 0·3027 | 1·3116 | 0·0680 | | |
| 2·00 | 1·2670 | 0·3026 | 1·3042 | 0·0496 | | |
| 2·50 | 1·2564 | 0·2948 | 1·2755 | 0·0424 | | |
| 3·00 | 1·2516 | 0·2859 | 1·2685 | 0·0413 | | |

The convergence of the eigen-frequency of the fastest-growing (or the principal) mode as the dimension of the matrix $M$ is increased, is shown in Table 3 for $m = 2$ (bisymmetric) perturbation in cold disk with $\alpha = 0{\cdot}25$ and $\beta = 1{\cdot}0$. It can be seen that the relative variations in the real and the imaginary parts of the eigen-value, $\omega$ defined by

$$\Delta\,\omega_r^{(i,j)} = \left|\frac{\omega_r^{(i)} - \omega_r^{(j)}}{\omega_r^{(i)}}\right|, \quad \Delta\,\omega_i^{(i,j)} = \left|\frac{\omega_i^{(i)} - \omega_i^{(j)}}{\omega_i^{(i)}}\right|$$

are fairly small. Here the superscripts denote the dimension of the matrices used. For instance, considering $i = 45$ and $j = 39$, one obtains $\Delta\,\omega_r = 1{\cdot}4 \times 10^{-4}$ and $\Delta\,\omega_i = 7 \times 10^{-2}$.

Fig. 3 compares the eigen-patterns for the principal mode with $m = 2$ as obtained from a 27 × 27 matrix and a 45 × 45 matrix. It can be noticed here that the patterns remain essentially unaltered by an increase in the size of the matrix considered, confirming thereby the proper convergence of the frequency, as well as the eigen-functions of the principal mode.

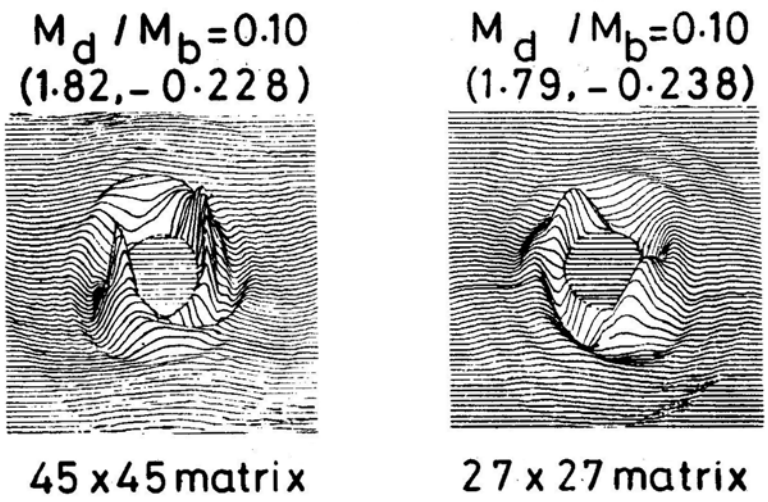


**Figure 3**. The bi-symmetnc ($m = 2$) principal (fastest-growing) eigen-mode as obtained by 27×27 and 45×45 matrices. Notice that the patterns are unaltered apart from a small rotational shift in resulting patterns.

**Table 4.** The convergence of various eigen-frequencies of the annular disk with the increase in the number of segments in the interval ($a$, $b$). $m = 2$, $a/b = 0{\cdot}25$, $M_d/M_b = 0{\cdot}5$, $c = 0$ (cold disk).

| No. of segments | 1 | | 2 | | 3 | |
|---|---|---|---|---|---|---|
| Eigen-mode | $\omega_r$ | $-\omega_i$ | $\omega_r$ | $-\omega_i$ | $\omega_r$ | $-\omega_i$ |
| I | 1·5231 | 0·2952 | 1·5229 | 0·2948 | 1·5231 | 0·2950 |
| II | 1·4748 | 0·0542 | 1·4743 | 0·0563 | 1·4745 | 0·0567 |
| III | 0·5820 | 0·0098 | 0·5801 | 0·0064 | 0·5800 | 0·0044 |
| IV | 1·0723 | 0·0161 | 1·0753 | 0·0052 | | |

Now, the matrix elements such as $P_{kj}$, $Q_{kj}$, which are certain integrated quantities over the disk, are obtained by using a 32-point Gaussian quadrature. To check the accuracy of the matrix elements themselves, we divide the interval ($\alpha$, 1) in more segments and then use the quadrature in each segment. The net quantities are obtained by summing up the contributions from each segment. Table 4 shows the allowed modes with $n_d = 1$, 2 and 3, where $n_d$ is the number of divisions in the interval ($\alpha$, 1). The relative errors for the first two modes are fairly small, while the two lower modes do not appear to be valid unstable modes of the system since the errors are large for them. We notice that as one adopts more accurate quadratures, these unstable modes disappear (*i.e.* stabilized) and do not yield spiral patterns. In our calculations, we have used $n_d = 3$.

In almost all the cases, we find that the principal mode shows a fairly smooth spiral pattern. We do not find any 'explosive' modes, with $\omega_i > \omega_r$, in our calculations. Also, there are no unstable modes in the disks with $\alpha = 0{\cdot}5$, $0{\cdot}75$ when $\beta < 0{\cdot}25$. Thus, massive bulge appears to suppress the unstable modes completely. A similar result is obtained by Hohl (1976) and Berman, Brownrigg and Hockney (1979) that bar instabilities are completely quenched in the presence of massive halo around the flat disk. We find here that the central spherical bulge also acts in a similar fashion. However, for the disks with $\alpha = 0{\cdot}25$ this is not the case even with the bulges as massive as 50 $M_d$ (*i.e.* $\beta \sim 0{\cdot}02$). Thus the suppression of the unstable modes is not efficient if the central bulge is confined to a smaller region. The pattern velocity ( $\equiv -\omega_i/m$) and the amplification rates ($\equiv \omega_i$) for the principal mode, with $m = 2$, are listed in Table 5. As the bulge decreases, the pattern velocity also decreases, which implies that the dominant pattern rotates slower in systems with smaller bulge content. On the other hand, the amplification rate decreases as the bulge increases (or $\beta$ decreases). However, in the disks with $0{\cdot}4 < \beta < 3{\cdot}0$ and $\alpha = 0{\cdot}25$, $\omega_i$ remains essentially constant.

**Table 5.** Convergence of eigenmodes with the increase in the dimension of the matrix $M$. $m = 2$, $c = 0$ (cold disk), $a/b = 0{\cdot}25$, $M_d/M_b = 1{\cdot}0$.

| Dimension of the truncated eigenmatrix | Principal mode | |
|---|---|---|
| | $\omega_r$ | $-\omega_i$ |
| 9 × 9 | 1·2727 | 0·2654 |
| 15 × 15 | 1·3481 | 0·3508 |
| 21 × 21 | 1·3591 | 0·3640 |
| 27 × 27 | 1·3617 | 0·3473 |
| 33 × 33 | 1·3625 | 0·3229 |
| 39 × 39 | 1·3631 | 0·2999 |
| 45 × 45 | 1·3650 | 0·2800 |

Fig. 4 shows the two armed patterns associated with the principal mode in the cold disks with $\alpha$ = 0·25 and with gradually increasing $\beta$. The spirals are smooth and tightly wrapped in the systems with massive bulge component (small $\beta$). It is noticed that the resulting patterns are strongly wrapped towards the central inner edge of the disk. However, as $\beta$ increases (or the bulge diminishes) the patterns open up and spread over the entire disk. Thus, we find here that the spiral patterns tend to be more open in the systems with smaller central bulge. Such a feature would, probably in a more rigorous study with the background population II stars in the disk, help the understanding of the transition of Sa $\rightarrow$ Sc galaxies.

Takahara (1978), Aoki, Noguchi and Iye (1979) and Ambastha and Varma (1981) pointed out that the global density waves in self-gravitating disks can be suppressed if the thermal energy (or pressure) is increased. In moderately warm disks, the snort wavelength (or the tightly wound) modes are significantly affected by the pressure. We obtain a similar result here in the case of disk-bulge systems also. Table 6

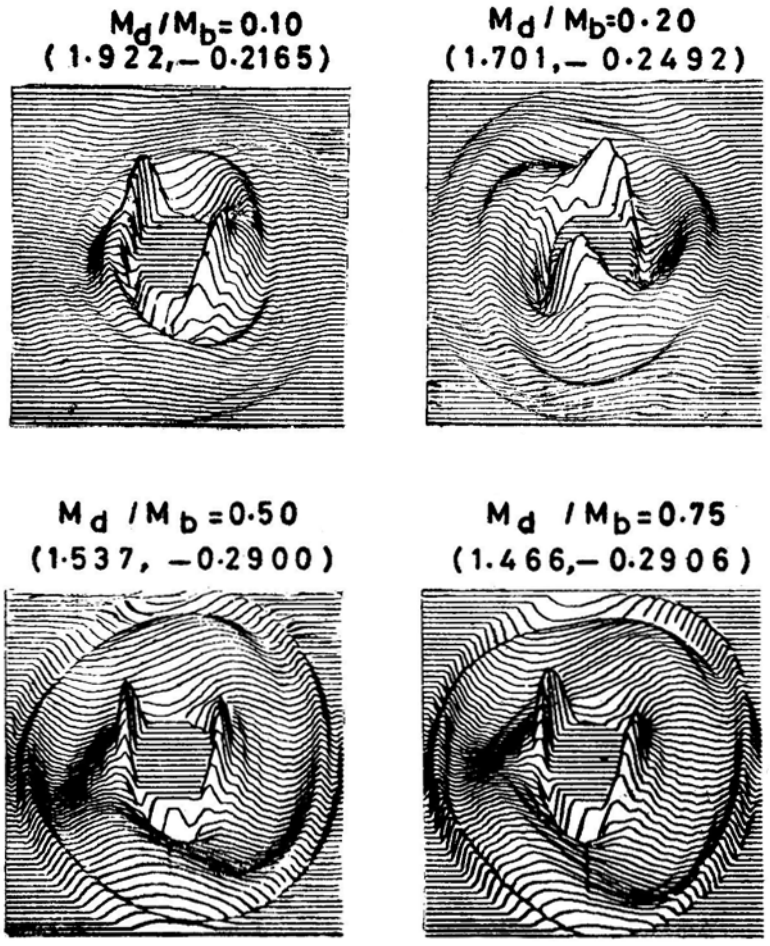


**Figure 4.** The bisymmetric ($m$ = 2) surface-density perturbation Patterns associated with the principal mode.The sequence exhibits the patterns in the disks with decreasing bulge mass.

**Table 6.** Effect of thermal pressure on unstable modes, ($m$ = 2), $M_d/M_b$ = 1·0, a/$b$ = 0·25.

| | I | | II | |
|---|---|---|---|---|
| $c$ | $\omega_r$ | $-\omega_i$ | $\omega_r$ | $-\omega_i$ |
| 0·000 | 1·3650 | 0·2820 | 1·3150 | 0·0774 |
| 0·001 | 1·3472 | 0·2633 | 1·3341 | 0·0813 |
| 0·002 | 1·3264 | 0·2457 | 1·3474 | 0·0848 |
| 0·003 | 1·3040 | 0·2321 | 1·3823 | 0·0853 |
| 0·004 | 1·2838 | 0·2223 | 1·4046 | 0·0819 |
| 0·005 | 1·2672 | 0·2140 | 1·4232 | 0·0766 |
| 0·006 | 1·2536 | 0·2057 | 1·4390 | 0·0706 |
| 0·007 | 1·2425 | 0·1968 | 1·4527 | 0·0643 |
| 0·008 | 1·2337 | 0·1873 | 1·4649 | 0·0580 |
| 0·009 | 1·2269 | 0·1772 | 1·4760 | 0·0516 |
| 0·010 | 1·2212 | 0·1667 | 1·4862 | 0·0450 |
| 0·015 | 1·2208 | 0·1152 | | |
| 0·020 | 1·2393 | 0·0741 | | |
| 0·025 | 1·2620 | 0·0327 | | |
| 0·030 | | | | |

shows the frequencies in. 'hot' disks for $\beta$ = 1·0, $\alpha$ = 0·25 and $m$ = 2. As the pressure (measured by the parameter $c$) increases, the amplification rate of the principal mode decreases and finally vanishes completely at $c$ = 0·03. The second unstable mode follows this trend at $c \gtrsim 0{\cdot}015$. Fig. 5 shows the pattern of oscillation associated with the density perturbations for the principal mode when $\beta$ = 1·0. $\alpha$ = 0·25 and $c$ = 0·002. We find that the peaks near the inner edge remain unchanged, whereas, the amplitude near the outer edge exhibits an abrupt jump.

In all cases, the eigen-patterns rotate in a clock-wise sense.

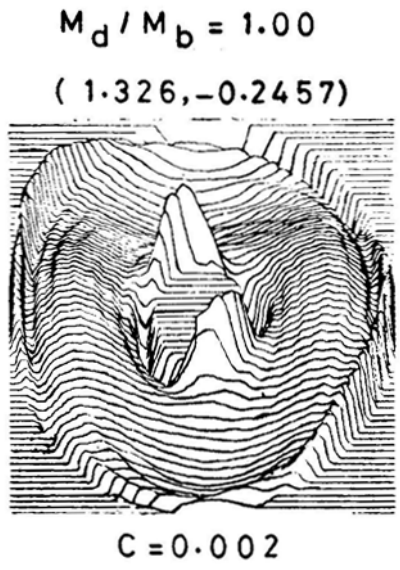


**Figure 5.** The principal bisymmetric mode in a hot disk, with the measure of 'hotness', $c$ = 0·002.

## 6. Conclusions

In all cold disks, there exist modes with large growth rates, which represent the 'explosive' or violent instabilities of the system. Such modes, however, cannot grow indefinitely, since the energy content of the disk is not infinite. Their growth would be affected by nonlinear effects and also by large halo enveloping the disk. We show here that such instabilities may not occur in the presence of massive central bulge of the galactic systems.

We find here some indications that the nature of the spiral patterns would depend on the disk-to-bulge ratio. The dominant mode shows a regular and smooth spiral pattern, which opens up and covers entire disk as the central bulge diminishes. This may, in some sense, explain the transition from Sa to Sc type as the amorphous bulge decreases in the galactic systems. There exist some modes with $\omega_i \ll \omega_r$ growing very slowly compared to the principal mode and show broken and ill-defined patterns, suggesting that the principal mode may dominate the system ultimately. However, only a nonlinear analysis governing the evolution of the system would resolve this problem.

It may be interesting to consider the possibility of the disk continuing inside the bulge. However, the bulge has been considered here as fixed and spherical in shape such that the potential contributed by it at a point, external to its surface, can simply be assumed as the potential of a point mass placed at the centre of the system. If the disk continues inside the bulge, the potential of the bulge has to be modified accordingly.

A study of the effect of various fixed population II distributions on the stability of the annular disks is being carried out.

## Acknowledgements

The computational work has been carried out on IBM 360/44 at the computer centre, Physical Research Laboratory.

## Appendix

We list here the expressions for the matrix elements constituting the infinite sub-matrices, $P$, $Q$, $R$ ... of the eigen-matrix, $M$:

$$M_j P_{kj} = \tfrac{1}{2}\,{}^{(m-1)}\mathbf{F}_{kj}^{(m-1)} + \tfrac{1}{2}\int_a^1 \xi\, V_0(\xi)\,(\lambda_j F_{j\xi}^m F_{k\xi}^{m-1} + \lambda_k F_{j\xi}^{m-1} F_{k\xi}^m)\, d\xi$$

$$- 2(m-1)\int_a^1 V_0(\xi)\, F_{j\xi}^{m-1} F_{k\xi}^{m-1}\, d\xi$$

$$M_j Q_{kj} = \tfrac{1}{2}\,{}^{(m-1)}\mathbf{F}_{kj}^{(m+1)} - \tfrac{1}{2}\int_a^1 \xi\, V_0(\xi)\,(\lambda_k F_{j\xi}^{m-1} F_{k\xi}^m - \lambda_j F_{j\xi}^m F_{k\xi}^{m-1})\, d\xi$$

$$M_j\, R_{kj} = c\,\gamma \int_\alpha^1 \xi\, \sigma_0^{\gamma-2}\,(\xi)\,\lambda_j\, F_{j\xi}^m\, F_{k\xi}^m\, d\xi - \frac{1}{\pi}\left(M_k\,\delta_{kj} + \frac{4}{\pi^2}\mathbf{I}_{kj}^{(1)}\right)$$

$$M'\, S_{kj} = -\tfrac{1}{2}\,{}^{(m+1)}\mathbf{F}_{kj}^{(m-1)} + \tfrac{1}{2}\int_\alpha^1 \xi\, V_0\,(\xi)\,(\lambda_j\, F_{j\xi}^m\, F_{k\xi}^{m-1} - \lambda_k\, F_{k\xi}^m\, F_{j\xi}^{m+1})\, d\xi$$

$$M_j'\, T_{kj} = -\tfrac{1}{2}\,{}^{(m+1)}\mathbf{F}_{kj}^{(m+1)} - 2\,(m+1)\int_\alpha^1 F_{j\xi}^{m+1}\, F_{k\xi}^{m+1}\, V_0\,(\xi)\, d\xi$$

$$+ \tfrac{1}{2}\int_\alpha^1 \xi\, V_0\,(\xi)\,(\lambda_j\, F_{j\xi}^m\, F_{k\xi}^{m+1} + \lambda_k\, F_{j\xi}^{m+1}\, F_{k\xi}^m)\, d\xi$$

$$M_j'\, U_{kj} = -\,c\,\gamma \int_\alpha^1 \xi\, \sigma_0^{\gamma-2}\,(\xi)\,\lambda_j\, F_{j\xi}^m\, F_{k\xi}^m\, d\xi + \frac{1}{\pi}\left(M_k'\,\delta_{kj} - \frac{4}{\pi^2}\mathbf{I}_{kj}^{(2)}\right)$$

$$M_j''\, V_{kj} = \tfrac{1}{2}\int_\alpha^1 \xi\, \sigma_0\,(\xi)\,\lambda_j\, F_{j\xi}^{m-1}\, F_{k\xi}^{m-1}\, d\xi$$

$$M_j''\, W_{kj} = -\tfrac{1}{2}\int_\alpha^1 \xi\sigma_0\,(\xi)\,\lambda_j\, F_{j\xi}^{m+1}\, F_{k\xi}^{m+1}\, d\xi$$

$$M_j''\, X_{kj} = -\,m\int_\alpha^1 V_0\,(\xi)\, F_{j\xi}^m\, F_{k\xi}^n\, d\xi$$

where, we have defined

$${}^{(m-1)}\mathbf{F}_{kj}^{(m-1)} = V_0\,(1)\, F_k^{m-1}\, F_j^{m-1} - V_0\,(\alpha)\, F_{k\alpha}^{m-1}\, F_{j\alpha}^{m-1}$$

$${}^{(m-1)}\mathbf{F}_{kj}^{(m+1)} = V_0\,(1)\, F_k^{m-1}\, F_{jk}^{m+1} - V_0\,(\alpha)\, F_{k\alpha}^{m-1}\, F_{j\alpha}^{m+1}$$

$${}^{(m+1)}\mathbf{F}_{kj}^{(m-1)} = V_0\,(1)\, F_k^{m+1}\, F_j^{m-1} - V_0\,(\alpha)\, F_{k\alpha}^{m+1}\, F_{j\alpha}^{m-1}$$

$${}^{(m+1)}\mathbf{F}_{kj}^{(m+1)} = V_0\,(1)\, F_k^{m+1}\, F_j^{m+1} - V_0\,(\alpha)\, F_{k\alpha}^{m+1}\, F_{j\alpha}^{m+1}$$

and

$$\mathbf{I}_{kj}^{(1)} = \int_0^\infty \frac{z^2 dz}{(\lambda_k^2 + z^2)\,(\lambda_j^2 + z^2)}\left[\frac{K_z^m}{Y_j^m}\left\{ z F_k^{m-1}\, I_z^m - z\alpha\, F_{k\alpha}^{m-1}\, I_{z\alpha}^m \right.\right.$$

$$\left.\left. - \frac{I_{z\alpha}^m}{Y_{j\alpha}^m}\left\{ z F_k^{m-1}\, K_z^m - z\alpha\, F_{k\alpha}^{m-1}\, K_{z\alpha}^m \right\} \right]\right.$$

$$\mathbf{I}_{kj}^{(2)} = \int_0^\infty \frac{z^2\,dz}{(\lambda_k^2+z^2)\,(\lambda_j^2+z^2)}\left[\frac{K_z^m}{Y_j^m}\left\{zF_k^{m+1}\,I_z^m - za\,F_{k_a}^{m+1}\,I_{z_a}^m\right\}\right.$$
$$\left. + \frac{I_{z_a}^m}{Y_{j_a}^m}\left\{zF_k^{m+1}\,K_z^m - za\,F_{z_a}^{m+1}\,K_{z_a}^m\right\}\right].$$

Also, $M_j$, $M'_j$ and $M''_j$ are defined as

$$M_j = -\tfrac{1}{2}\,[F_j^{m-1}\,F_j^{m-1} - F_{j_a}^{m-1}\,F_{j_a}^{m-1}]$$

$$M'_j = -\tfrac{1}{2}\,[F_j^{m+1}\,F_j^{m+1} - F_{j_a}^{m+1}\,F_{j_a}^{m+1}]$$

$$M''_j = -\tfrac{1}{2}\,[F_j^{m+1}\,F_j^{m-1} - F_{j_a}^{m+1}\,F_{j_a}^{m-1}].$$

In all the above expressions, we have represented Bessel's functions, for brevity, as

$F_{j_a}^m \rightarrow F_m\,(\lambda_j\,a)$, *etc.*

## References


Ambastha, A. 1981, *Ph D thesis*, Physical Research Laboratory, Ahmedabad.
Ambastha, A., Varma, R. K. 1978, *Astrophys. Sp. Sci*., **55,** 459.
Ambastha, A., Varma, R. K. 1981, Preprint.
Aoki, S., Noguchi, M., Iye, M. 1979, *Publ. astr. Soc. Japan*, 31, 737.
Berman, R. H., Brownrigg, D. R. K., Hockney, R. W. 1978, *Mon. Not. R. astr. Soc*, **185,** 861.
Bertin, G. 1980, *Phys. Rep*., **61,** 1.
Bertin, G., Mark, J. W.-K. 1978, *Astr. Astrophys*., **64,** 389.
Clutton-Brock, M. 1972, *Astrophys. Sp. Sci.*, **16,** 101.
Freeman, K. C. 1970, *Astrophys. J*., **160,** 811.
Gordon, M. A., Burton, W. B. 1976, *Astrophys. J*., **208**, 346.
Hart, L., Pedlar, A. 1976, *Mon. Not. R. astr. Soc.*, **176,** 547.
Hohl, F. 1976, *Astr. J*., **81,** 30.
Iye, M. 1978, *Publ, astr. Soc. Japan*, **30**, 223.
Kato, S. 1970, *Publ. astr. Soc. Japan*, **22,** 285.
Kodaira, K. 1974, *Publ. astr. Soc. Japan*, **26,** 255.
Lin, C. C., Shu, F. H. 1964, *Astrophys. J*., **140,** 646.
Lin, C. C., Shu, F. H. 1966, *Proc nat. Acad. Sci. Am*., 55, 229.
Lin, C. C, Yuan, C, Shu, F. H. 1969, *Astrophys. J*., **155,** 721.
Lynden-Bell, D., Ostriker, J. P. 1967, *Mon. Not. R. astr. Soc.*, **136,** 293.
Mark, J. W.K. 1977, *Astrophys. J*., **212**, 645.
Norman, C. A. 1978, *Mon. Not. R. astr. Soc.*, **182,** 457.
Pannatoni, R. F., Lau, Y. Y. 1979, *Proc nat. Acad. Sci. Am*., **76,** 4.
Sandage, A., Freeman, K. C., Stokes, N. R. 1970, *Astrophys. J*., **160,** 831.
Shu, F. H. 1970, *Astrophys. J.,* **160,** 89.
Stecker, F. W. 1976, GSFC Report X-662-76-154, 357.
Takahara F. 1978, *Publ. astr. Soc. Japan,* **30**, 253.
Toomre, A. 1969, *Astrophys. J*., **158,** 899.
Yabushita, S. 1969, *Mon. Not. R. astr. Soc*., **142,** 201.